APPLIED SCIENCES AND ENGINEERING

A water lily–inspired hierarchical design for stable and efficient solar evaporation of high-salinity brine

Ning Xu*, Jinlei Li*, Yang Wang, Chang Fang, Xiuqiang Li, Yuxi Wang, Lin Zhou, Bin Zhu, Zhen Wu, Shining Zhu, Jia Zhu†

In recent years, interfacial solar vapor generation has shown great potential in realizing desalination and wastewater treatment with high energy conversion efficiency. However, high evaporation rate cannot be maintained because of the seemingly unavoidable fouling or salt accumulation on the solar absorbers. The degradation accelerates as the solute concentration increases. Here, we demonstrate a water lily–inspired hierarchical structure that enables efficient evaporation (~80% solar-to-vapor efficiency) out of high-salinity brine [10 weight % (wt %)] and wastewater containing heavy metal ions (30 wt %). More notably, neither decrease in evaporation rate nor fouling on absorbers was observed during the entire evaporation process until water and solute were completely separated. With the capabilities of stable and high-rate evaporation out of high-salinity brine and the effective separation of solute from water, it is expected that this technology can have direct implications in various fields such as wastewater treatment, sea-salt production, and metal recycling.

INTRODUCTION

Freshwater scarcity has become one of the most serious global challenges we face today, as the advancements of human civilization lead to substantial consumption and contamination of fresh water. Therefore, various technologies of water treatment, such as reverse osmosis (RO) (*1*, *2*) and ultrafiltration (*3*, *4*), have been developed to alleviate the pressure from freshwater withdrawal and to reduce the environmental impact of discharged wastewater. Zero liquid discharge (ZLD), the complete separation of solute and water for reuse to minimize harmful ecological impacts, is proposed as an ultimate goal of wastewater treatment (*5*). However, so far, the lack of an energy-efficient and cost-effective way to treat concentrated brine [over 7 weight % (wt %)] has been a major roadblock for large-scale implementation of ZLD (*5*–*8*). As the brine concentration increases, the pressure (energy) required to drive the filtering process in mainstream technologies (such as RO) increases dramatically (*6*–*8*) at the same time, the service life of these membranes is shortened significantly (*6*–*8*) the result is the high cost of water treatment. Therefore, it is imperative to explore new pathways for treating water, particularly for high-concentration brine or wastewater, and to realize complete separation of water and solute with minimized cost in energy and to the environment.

In recent years, interfacial solar vapor generation has attracted intensive attention because of the fast solar-driven evaporation and minimum carbon footprint when treating seawater or wastewater (*9*–*33*). However, so far, its high evaporation rate cannot be maintained and usually decreases very quickly, particularly when treating a highly concentrated water source (brine or wastewater). The fundamental paradox between high-rate evaporation and long-term stability of interfacial solar evaporation can be understood as follows. The key for interfacial solar evaporation to achieve high energy conversion efficiency and therefore high evaporation rate is that substantial amount of absorbed solar energy needs to be concentrated into a small volume of water molecules, typically confined within porous solar absorbers. As water evaporates very quickly, the salt or solute will be left behind, accumulating and/or crystalizing at the evaporation site of solar absorbers (fig. S1). This accumulation of salt/solute, sometimes referred to as fouling, blocks out sunlight and plugs interior channels for water supply and vapor escape, which significantly degrades the performance of solar evaporation. With the increased salt concentration of brine, the salt will accumulate much more quickly on the surface of absorbers as water evaporates, leading to more severe fouling issues, accelerated decrease of evaporation rate, and the eventual collapse of devices.

Several strategies have been explored to maintain the high evaporation rate over a long period out of concentrated brine. For example, inspired by mangrove trees, Mi *et al.* (*34*) developed "artificial leaves" relying on salt secretion to treat brine with high salinity. Despite the exciting progress, there is still a notable decrease in evaporation rate (~25% decline for 15 wt % saline water). Another strategy is to increase the water supply to the absorbers to dissolve away the salt (*35*, *36*). However, more water supply not only dissolves away the salt but also carries away the energy, leading to increased heat loss and reduced efficiency. Recently, several studies designed separate structures/units for capturing sunlight and collecting the remaining salt during desalination. By carefully dividing the area for sunlight absorption and that for salt deposition on an integrated evaporator, Wang *et al.* (*22*) realized a solar desalination with relatively stable performance over 120 hours. Chen's group creatively proposed a contactless solar evaporation structure, which physically separates the absorber and water, and achieved contamination resistance for the absorber over a long time span (*37*). Yet, the realized energy conversion efficiency of 24.6% under 1-sun illumination still has much room for further improvement (*37*).

Water lily naturally (Fig. 1A) has an elegant system of transpiration with several features. First, the upper epidermis absorbs sunlight and provides stomata for water vapor escape. Its well-known hydrophobic surface has self-cleaning property. Second, the water lily can float naturally on the surface of water because of the existence of lacunae (air chamber) at the bottom of the leaf. Third, there exists a confined water path provided by vascular bundles to pump up water and

National Laboratory of Solid State Microstructures, College of Engineering and Applied Sciences, Jiangsu Key Laboratory of Artificial Functional Materials, Nanjing University, Nanjing 210093, P. R. China.
*These authors contributed equally to this work.
†Corresponding author. Email: jiazhu@nju.edu.cn

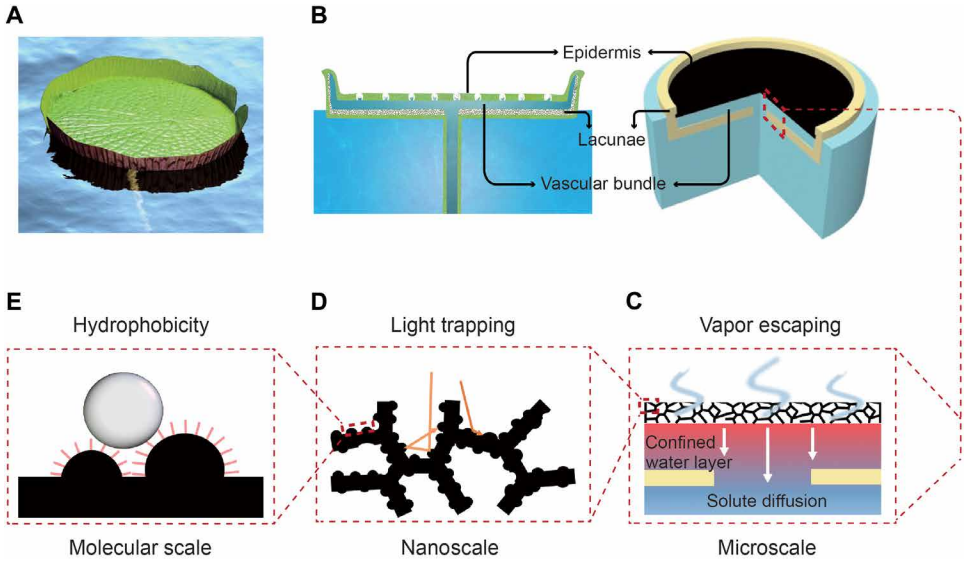

Fig. 1. Design concept of the water lily–inspired hierarchical structure. (**A** and **B**) Water lily and water lily–inspired design for solar vapor generation, respectively. They share several key features: the upper epidermis with hydrophobic surface absorbs the sunlight and provides stomata for water vapor escape, lacunae (air chamber) at the bottom of the leaf keep a water lily afloat on the water, and vascular bundles (water path) provide a confined water supply. (**C**) Microscale schematic of a confined water layer sandwiched between the hydrophobic top solar absorber and the bottom stand with low thermal conductivity. Evaporation occurs at the water surface below the absorber, and salt/solute is excreted by the water path, avoiding accumulation/crystallization of solute on the absorber. (**D**) Nanoscale light trapping for the top solar absorber. (**E**) Molecular-scale surface modification for the hydrophobic surface of the top solar absorber.

then spread it into the large surface of the water lily. Taking advantage of these features, we propose a water lily–inspired hierarchical structure (WHS), which can realize highly efficient, stable solar evaporation in high-salinity brine/wastewater until complete separation of water and solute is obtained.

The WHS device we designed consists of a top solar absorber and a bottom stand. Different from most, if not all, of the previous studies, water cannot get into the absorber, but form a thin water layer sandwiched between the top hydrophobic absorber and the bottom stand (Fig. 1B). This thin water layer is the key to achieving stable and efficient solar evaporation out of highly concentrated brine. The solar evaporation is efficient because the absorbed solar energy will be concentrated into this thin layer of water for evaporation, enabling interfacial-type solar evaporation. The nanoscale light trapping and the confined water supply minimize the loss of light absorption and heat conduction, respectively. The solar evaporation is also stable even when treating highly concentrated brine, because unlike previous designs of interfacial solar evaporation, the thin layer of water for solar evaporation is formed below the absorber rather than within the absorber. Therefore, as water evaporates, salt/solute will not accumulate on the surface of the absorber, as in the case of most previous interfacial solar evaporation. Rather, salt/solute will be excreted downward with the water in one-dimensional channels. Therefore, this design can enable fast and stable evaporation when treating very high–salinity brine and high-concentration wastewater, realizing complete separation of water and solute, as demonstrated below.

The WHS device also has similar features to water lily (Fig. 1B). First, the top solar absorber is hierarchically designed to absorb the sunlight while providing artificial "stomata" for continuous vapor escape (Fig. 1C). The hierarchical design is essential for achieving both functions of light absorption and vapor escape. Nanoscale light trapping is the key for efficient light absorption (*38*, *39*) (Fig. 1D), while micrometer-sized pores provide pathways for vapor escape. In addition, nanostructures of the absorber with molecular-scale surface modification endow the surface of solar absorber with hydrophobic properties (Fig. 1E), mimicking the hydrophobic surface of water lily. The hydrophobic surface ensures that water does not get into the absorber, which is critical for efficient and stable solar evaporation. Second, similar to the function of the lacunae (air chamber) of water lily, a bottom stand supports the entire structure to float naturally on water surface. This bottom stand also serves as a thermal insulation layer for minimizing heat losses (fig. S2). At last, just like a water lily, water can only come up through confined channels, that is, through-holes of the bottom stand.

RESULTS AND DISCUSSION

Fabrication and characterization of WHS

As explained above, the top solar absorber as the pivotal part of WHS needs to have micrometer-sized pores for vapor escape, nanoscale light trapping for efficient solar absorption, and hydrophobicity for antifouling ability. In addition, as the evaporation happens below the top solar absorber, it will be ideal for the solar absorber to have high thermal conductivity for effective transfer of absorbed solar energy to water surface. Therefore, copper foam was chosen here as the initial substrate for the fabrication of the absorber for two reasons (Fig. 2A): It has a high thermal conductivity of 34.1 W m^{-1} K^{-1} (fig. S3), and it contains micrometer-sized pores for vapor escaping (Fig. 2B). To enhance solar absorption via nanoscale light trapping effect (*37*, *38*), the original smooth surface of the Cu foam (Fig. 2C) was transformed into knife-like nano-plates by chemical etching (Fig. 2D). The surface of the absorber was then coated with a layer of Al_2O_3 [the scanning electron microscopy (SEM) image of which is shown in fig. S4] and decorated with carbon black (CB) nanoparticles (Fig. 2E) to protect the surface and enhance sunlight absorption at

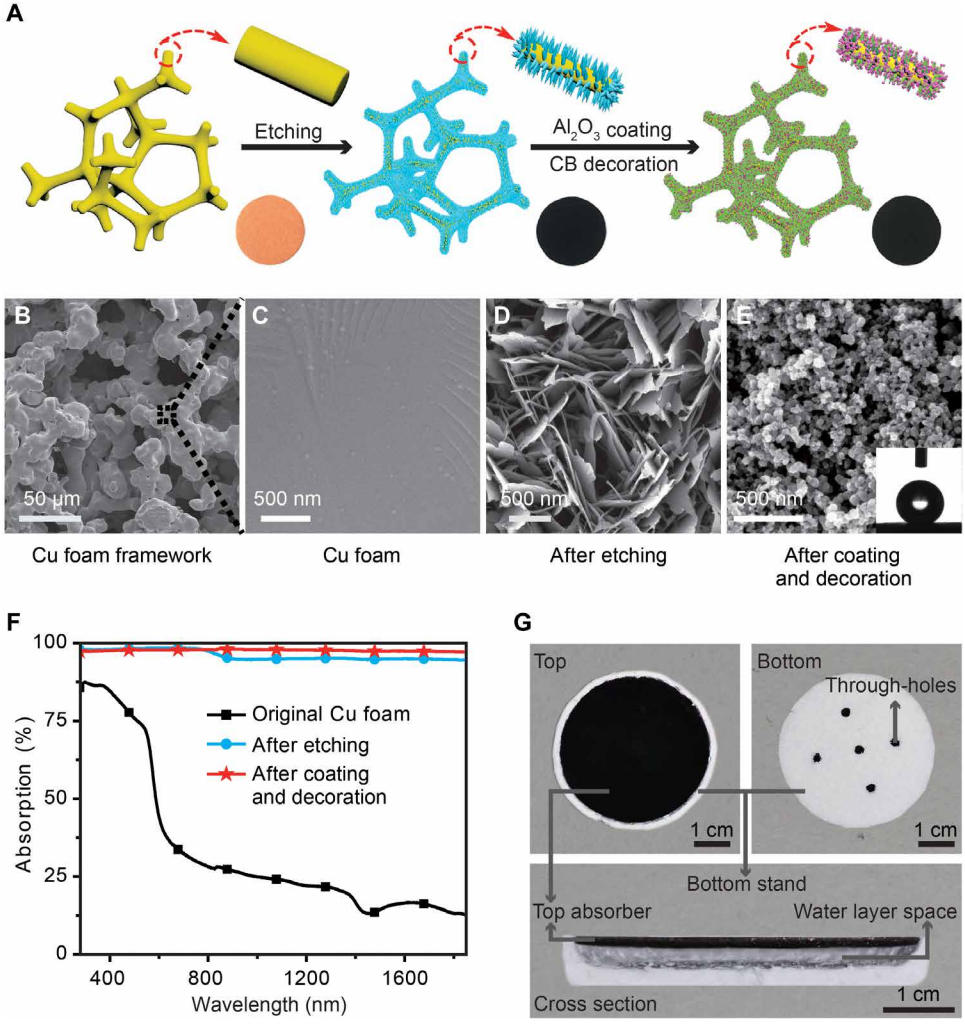

Fig. 2. Fabrications and characterizations of a WHS. (**A**) Schematics of the fabrication processes of the top solar absorber. From left to right: the original Cu foam, after chemical etching, after Al_2O_3 coating, and subsequent carbon black (CB) decoration. The insets show optical photographs of the absorber at different fabricating stages. (**B**) Scanning electron microscopy (SEM) images of the Cu foam with micrometer-sized pores. (**C** to **E**) High-resolution SEM images of the absorber at different process stages: surface of the original Cu foam (C), after etching (D), and after Al_2O_3 coating and CB decoration (E). Inset of (E): contact angle of the absorber. (**F**) Absorption spectra of the absorber at different fabricating steps. From top to bottom: the original Cu foam, after etching, and after atomic layer deposition (ALD) coating and CB decoration. (**G**) Photographs of the top, bottom, and cross-sectional views for the WHS. The through-holes of the bottom stand provide the water supply. The diameter of the absorber is 4 cm.

infrared (IR), respectively (see fig. S5 and table S1 for more analyses). Figure 2F suggests that the absorber achieves ~98% sunlight absorption (from 280 to 1850 nm) after all the fabrication steps. The nanostructures on the absorber also enable the hydrophobicity of the absorber to be enhanced by molecular-scale surface modification (inset of Fig. 2E) (*40*), which is important to prevent water from entering the absorber (see Materials and Methods for more details about fabrication).

A bottom stand should have low density for floating, low thermal conductivity for heat localization, and through-holes for confined water supply (see fig. S6 for more details). Polystyrene with a low thermal conductivity of <0.04 W m^{-1} K^{-1} was used to fabricate the bottom stand (Fig. 2G). The surface ratio of holes over the bottom stand was designed to be 1:40 for heat localization, as well as for effective water supply and excretion of salt/solute. The finished bottom stand was assembled beneath the prepared top solar absorber, forming the integrated WHS (Fig. 2G).

Efficiency and utility

To evaluate the evaporation performance of the WHS, deionized (DI) water, 10 wt % brine (see fig. S7 for performances under different salinities), and 30 wt % wastewater (a heavy metal solution with 20 wt % $NiCl_2{\cdot}6H_2O$ and 10 wt % $PdSO_4{\cdot}8/3H_2O$) were treated under 1-sun illumination (the evaporation curves are shown in fig. S8). As shown in Fig. 3A, evaporation rates (together with energy conversion efficiencies) of the DI water, 10 wt % brine, and 30 wt % wastewater are calculated to be 1.31 kg m^{-2} $hour^{-1}$ (79.8%), 1.28 kg m^{-2} $hour^{-1}$ (78.5%), and 1.27 kg m^{-2} $hour^{-1}$ (77.2%), respectively, comparable to the high-performance solar absorber reported previously (*9*, *11*).

To evaluate the purification effect of desalination and wastewater treatment by the WHS, the ion concentrations in purified water were carefully tracked (see fig. S9 for the details of water collection). It is found that the concentrations of all the primary ions in seawater

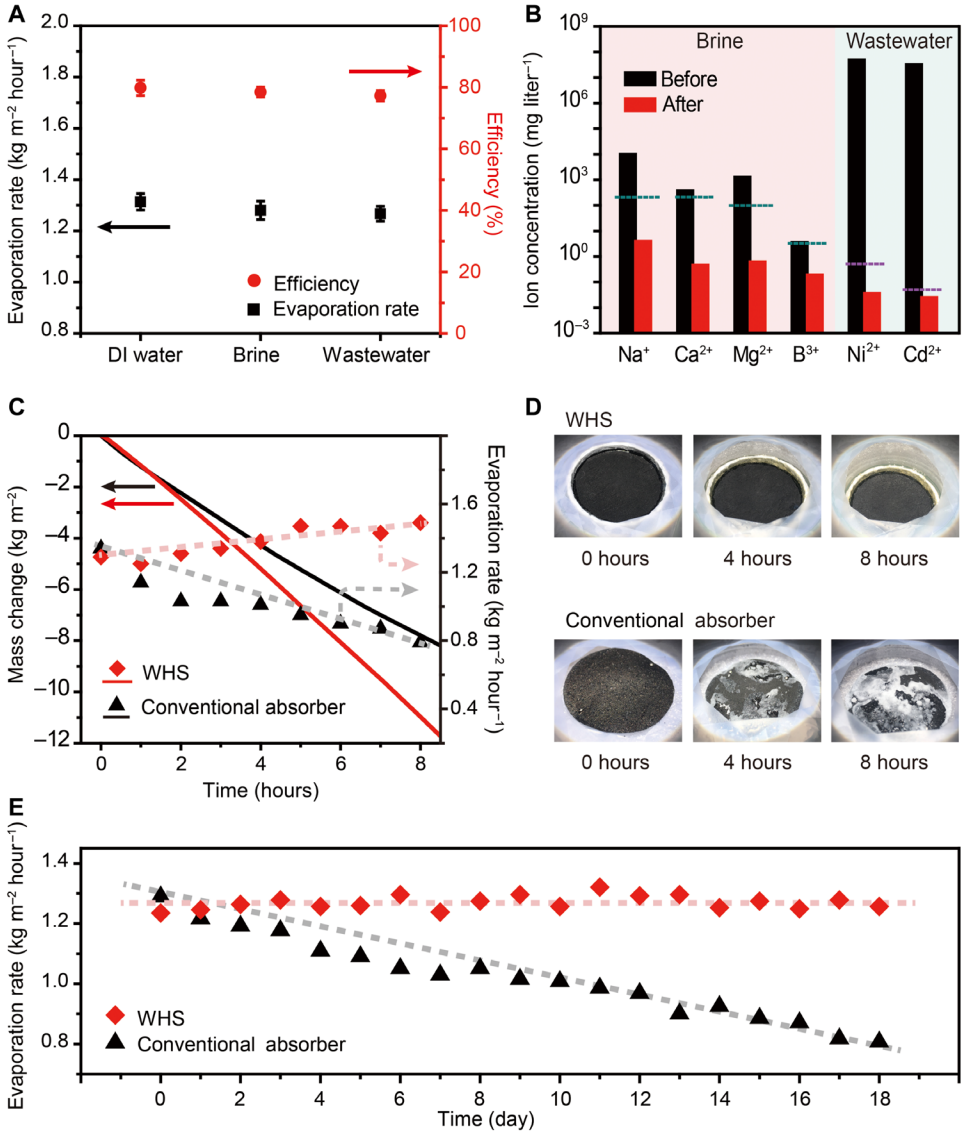

Fig. 3. Performance of solar-vapor generation. (**A**) Evaporation rates and energy conversion efficiencies of WHS for DI water, 10 wt % brine, and 30 wt % wastewater. (**B**) Ion concentrations before and after water purification. Seawater (collected from the Bohai Sea, China, with an average salinity of ~1 wt %) and wasterwater (with heavy metal ions, Ni^{2+} and Cd^{2+}) were used as water sources. The dashed blue lines and dashed violet lines show the WHO standard of ion concentrations for drinking water and standard for discharge, respectively. (**C**) Mass changes and evaporation rates of the WHS and a conventional solar absorber over 8 hours. Brine (10 wt %) was used as the water source. The evaporation rates out of pure water are also listed at 0 hours for comparison. (**D**) Photographs of the WHS and a conventional solar absorber over time when treating brine with 10 wt % salinity initially. (**E**) Outdoor solar evaporation performance of the WHS and a conventional solar absorber over 18 days when treating brine with 10 wt % salinity (photo credit: Ning Xu, Nanjing University).

(Na^+, Mg^{2+}, Ca^{2+}, and B^{3+}) and wastewater (Ni^{2+} and Cd^{2+}) or Na^+ in the brine with different salinity (fig. S10) are significantly reduced, meeting the World Health Organization (WHO) standard for drinking water or standard for discharge, respectively (Fig. 3B) (*41*, *42*).

Long-term stability

To examine whether the WHS can avoid performance degradation and the fouling issue, we performed a continuous 8-hour experiment of solar water treatment under a solar simulator (94043A, Newport) (see more details in Materials and Methods). The WHS and a conventional solar absorber with a similar solar evaporation rate out of pure water are chosen for fair comparison. As shown in Fig. 3C, during the continuous solar desalination under 1-sun illumination for 8 hours, the mass change of brine (10 wt % salinity) with the WHS almost evolves linearly, and the evaporation rates are maintained at a high level. The slight increase of evaporation rates can be attributed to the increase of water temperature during a long-duration test. In comparison, for the conventional solar absorber (see figs. S11 and S12 for fabrication and characterizations) under the same testing conditions, there is a clear decrease in evaporation rates over time. The average evaporation rate of the WHS over 8 hours is calculated to be 1.39 kg m^{-2} $hour^{-1}$, much higher than that of the conventional solar absorber (0.97 kg m^{-2} $hour^{-1}$).

During this test of treating 10 wt % brine over 8 hours, the surfaces of the WHS and the conventional solar absorber also behave very differently. The surface of the WHS remains clean during the entire evaporation (Fig. 3D), indicating great antifouling ability. However, for the conventional solar absorber, salt progressively accumulated on the surface (Fig. 3D), blocking sunlight absorption (energy input). This can also be verified by the temperature distributions of the absorbers, revealed by the IR images of the conventional solar absorber (fig. S1). The temperature of the surface area with fouling (salt accumulation) during the evaporation process is obviously lower than that without fouling, suggesting less sunlight absorption due to higher reflection of salt (*43*). In contrast, the temperature of the absorber in WHS is uniformly distributed (fig. S1), confirming that no fouling occurred.

We further performed an outdoor experiment of solar water treatment, treating brine (initially 10 wt % salinity) under natural sunlight over 18 days. As shown in Fig. 3E, the evaporation rate of WHS is found to be stable over 18 days, showing an average evaporation rate of 1.27 kg m^{-2} $hour^{-1}$. However, for the conventional solar absorber, evaporation rate decreased very quickly, over 30% drop in 18 days (fig. S13).

Complete separation of water and solute

More notably, the WHS can further enable solar evaporation until complete separation of water and solute is achieved when treating brine (10 wt %) and wastewater (30 wt % heavy metal solution). The photographs (first row) in Fig. 4 (A and B) demonstrate that, as the WHS floats on the surface of water, when water progressively evaporated out of brine/wastewater, the WHS moved downward day by day until water had completely evaporated and only salt/solute was left. Notably, the WHS exhibits efficient and stable evaporation performances (Fig. 4, A and B), and no fouling (salt or solute accumulation) was observed on the surfaces (second row in Fig. 4, A and B) during the entire process. The remaining salt/solute (crystal of NaCl and $NiCl_2{\cdot}6H_2O$ along with $PdSO_4{\cdot}8/3H_2O$) can be easily taken out after complete water evaporation, as shown in the insets in Fig. 4 (A and B, bottom right).

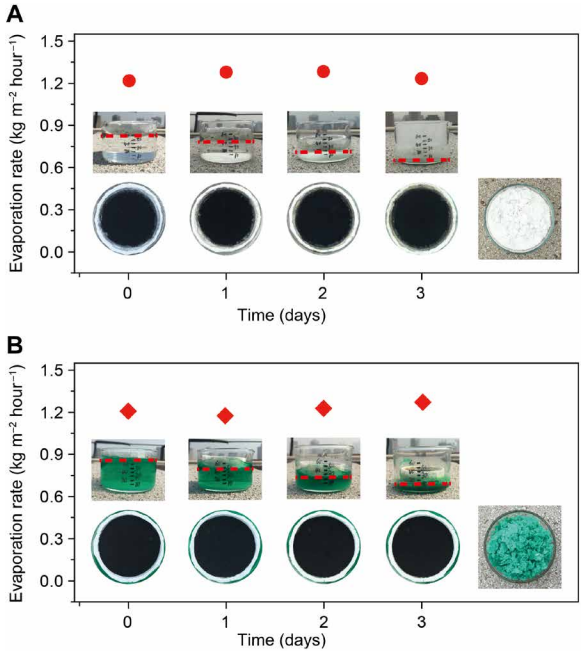

Fig. 4. Complete separation of water and solute after stable and efficient solar evaporation. (**A** and **B**) Evolutions of evaporation rates over time for solar desalination and wastewater treatment, respectively. Insets show the time-dependent photographs of the devices for outdoor solar desalination (A) and wastewater treatment (B). Side views/top views of the device are presented in the first row/second row, respectively (the dashed red lines indicate the bottom of the WHS). Photographs of recycled salt and solute are presented on the bottom right of (A) and (B), respectively (photo credit: Ning Xu, Nanjing University).

CONCLUSION

In conclusion, we demonstrated a WHS that can enable fast and stable evaporation over long term even when treating high-salinity brine or highly concentrated wastewater. Moreover, complete separation of water and solute is achieved without any fouling (salt or solute accumulation) observed in the device. It is expected that this WHS device, that is capable of efficient and effective separation of water and solute, will have direct implications not only in brine/wastewater treatment but also in various other fields, such as sea-salt production, resource recovery, and chemical fractionation.

MATERIALS AND METHODS

Fabrication of WHS

Copper foam (with a pore diameter of 20 to 50 μm and a thickness of 1 mm) was used for fabricating the top solar absorber. The nanostructures on the surface of the Cu foam were prepared by immersing the Cu foam into the mixture of $NaClO_2$, NaOH, $Na_3PO_4{\cdot}12H_2O$, and DI water (3.75:5:10:100 wt %) at ~95°C for 10 min. The surface of the sample was then coated by Al_2O_3 of 20 nm via atomic layer deposition (ALD), dip-coated with CB nanoparticles, and surface-modified with the solution of 1*H*,1*H*,2*H*,2*H*-perfluorooctyltrichlorosilane dissolved in methyl alcohol with a concentration of 2 volume %. The bottom stand was made of a thermally insulated polystyrene foam with drilled through-holes.

Experimental setup for solar desalination

A solar simulator (94043A, Newport) equipped with an optical filter for the standard AM 1.5G spectrum was used as the illuminant for all indoor experiments of solar desalination and wastewater treatment. During these experiments, the indoor temperature and humidity were carefully controlled to 27 to 28°C and ~30%, respectively. The mass change of water, later used for determining the evaporation rate together with the efficiency, was measured in real-time by a high-accuracy balance (FA 2004, 0.1 mg in accuracy).

Characterization

The microscopic structures of the absorbers were characterized by a scanning electron microscope (FEI Strata, Dual-beam FIB 235). The absorption spectra of the absorbers were measured by ultraviolet-visible spectroscopy (UV-3600, Shimadzu) attached with an integrating sphere (ISR-3100). A surface tension/contact angle meter (GBX Digidrop) was used to test the water contact angle of the sample. The thermal diffusivity (α) and specific heat (*c*) of the absorber were measured by using a NETZSCH LFA457 instrument in argon atmosphere. A Reineisen sample (Ø12.7 mm by 1.98 mm) was used as a standard at room temperature. Thermal conductivity was then calculated by

$\lambda = \alpha\rho c$, in which ρ is the density of the absorber. To evaluate the water purification effect of the WHS device, we collected the vapor via the setup in fig. S9. The concentrations of cations in condensed vapor were examined by ICP-OES (PerkinElmer Instruments, PTIMA 5300 DV). The IR images of the absorber surface were captured by an IR camera (FLUKE, Tix 580). The IR emittance spectra of the solar absorbers were measured by a Fourier transform IR spectrometer (Nicolet iS50, Thermo Fisher Scientific).

SUPPLEMENTARY MATERIALS

Supplementary material for this article is available at http://advances.sciencemag.org/cgi/content/full/5/7/eaaw7013/DC1

Fig. S1. Photographs and IR photographs of the conventional absorber and the WHS device after working for 8 hours.
Fig. S2. Heat localization in WHS.
Fig. S3. Thermal properties for the top solar absorber of the WHS.
Fig. S4. SEM image of the Cu foam after etching and Al_2O_3 coating.
Fig. S5. IR emittance spectra of the absorbers after Al_2O_3 coating and CB decoration.
Fig. S6. The mechanism of water supply for the WHS device.
Fig. S7. Vapor generation performances of the WHS treating brine with different salinities.
Fig. S8. Mass changes of different water sources over time with the WHS device.
Fig. S9. The schematic of the setup used for collecting purified water.
Fig. S10. Salinities of different brine before (3.5 wt %, 5 wt %, and 10 wt %) and after purification.
Fig. S11. The schematic of the conventional solar absorber.
Fig. S12. Characterizations of the conventional solar absorber.
Fig. S13. Performances of solar evaporation for the WHS device and conventional solar absorber at the beginning (0 day) and after 18 days of working.
Fig. S14. Concentrations of ions in the water before and after purification.
Table S1. Comparison of optical performances of the absorbers after Al_2O_3 coating and CB decoration.

REFERENCES AND NOTES

1. A. Alsheghri, S. A. Sharief, S. Rabbani, N. Z. Aitzhan, Design and cost analysis of a solar photovoltaic powered reverse osmosis plant for masdar institute. *Energy Procedia* **75**, 319–324 (2015).
2. S. M. Shalaby, Reverse osmosis desalination powered by photovoltaic and solar Rankine cycle power systems: A review. *Renew. Sustain. Energy Rev.* **73**, 789–797 (2017).
3. X. Fan, Y. Tao, L. Wang, X. Zhang, Y. Lei, Z. Wang, H. Noguchi, Performance of an integrated process combining ozonation with ceramic membrane ultra-filtration for advanced treatment of drinking water. *Desalination* **335**, 47–54 (2014).
4. R. Gopal, S. Kaur, Z. Ma, C. Chan, S. Ramakrishna, T. Matsuura, Electrospun nanofibrous filtration membrane. *J. Membr. Sci.* **281**, 581–586 (2006).
5. T. Tong, M. Elimelech, The global rise of zero liquid discharge for wastewater management: Drivers, technologies, and future directions. *Environ. Sci. Technol.* **50**, 6846–6855 (2016).
6. P. J. J. Alvarez, C. K. Chan, M. Elimelech, N. J. Halas, D. Villagrán, Emerging opportunities for nanotechnology to enhance water security. *Nat. Nanotechnol.* **13**, 634–641 (2018).
7. D. Jassby, T. Y. Cath, H. Buisson, The role of nanotechnology in industrial water treatment. *Nat. Nanotechnol.* **13**, 670–672 (2018).
8. M. Elimelech, W. A. Phillip, The future of seawater desalination: Energy, technology, and the environment. *Science* **333**, 712–717 (2011).
9. H. Ghasemi, G. Ni, A. M. Marconnet, J. Loomis, S. Yerci, N. Miljkovic, G. Chen, Solar steam generation by heat localization. *Nat. Commun.* **5**, 4449 (2014).
10. Y. Ito, Y. Tanabe, J. Han, T. Fujita, K. Tanigaki, M. Chen, Multifunctional porous graphene for high-efficiency steam generation by heat localization. *Adv. Mater.* **27**, 4302–4307 (2015).
11. X. Li, W. Xu, M. Tang, L. Zhou, B. Zhu, S. Zhu, J. Zhu, Graphene oxide-based efficient and scalable solar desalination under one sun with a confined 2D water path. *Proc. Natl. Acad. Sci. U.S.A.* **113**, 13953–13958 (2016).
12. L. Zhang, B. Tang, J. Wu, R. Li, P. Wang, Hydrophobic light-to-heat conversion membranes with self-healing ability for interfacial solar heating. *Adv. Mater.* **27**, 4889–4894 (2015).
13. L. Zhou, Y. Tan, J. Wang, W. Xu, Y. Yuan, W. Cai, Z. Zhu, J. Zhu, 3D self-assembly of aluminium nanoparticles for plasmon-enhanced solar desalination. *Nat. Photon.* **10**, 393–398 (2016).
14. C. Chen, Y. Li, J. Song, Z. Yang, Y. Kuang, E. Hitz, C. Jia, A. Gong, F. Jiang, J. Y. Zhu, B. Yang, J. Xie, L. Hu, Highly flexible and efficient solar steam generation device. *Adv. Mater.* **29**, 1701756 (2017).
15. Y. Li, T. Gao, Z. Yang, C. Chen, W. Luo, J. Song, E. Hitz, C. Jia, Y. Zhou, B. Liu, B. Yang, L. Hu, 3D-printed, all-in-one evaporator for high-efficiency solar steam generation under 1 sun illumination. *Adv. Mater.* **29**, 1700981 (2017).
16. L. Cui, P. Zhang, Y. Xiao, Y. Liang, H. Liang, Z. Cheng, L. Qu, High rate production of clean water based on the combined photo-electro-thermal effect of graphene architecture. *Adv. Mater.* **30**, e1706805 (2018).
17. F. Zhao, X. Zhou, Y. Shi, X. Qian, M. Alexander, X. Zhao, S. Mendez, R. Yang, L. Qu, G. Yu, Highly efficient solar vapour generation via hierarchically nanostructured gels. *Nat. Nanotechnol.* **13**, 489–495 (2018).
18. L. Zhu, M. Gao, C. K. N. Peh, X. Wang, G. W. Ho, Self-contained monolithic carbon sponges for solar-driven interfacial water evaporation distillation and electricity generation. *Adv. Energy Mater.* **8**, 1702149 (2018).
19. L. Zhu, M. Gao, C. K. N. Peh, G. W. Ho, Solar-driven photothermal nanostructured materials designs and prerequisites for evaporation and catalysis applications. *Mater. Horiz.* **5**, 323–343 (2018).
20. X. Zhou, F. Zhao, Y. Guo, Y. Zhang, G. Yu, A hydrogel-based antifouling solar evaporator for highly efficient water desalination. *Energ. Environ. Sci.* **11**, 1985–1992 (2018).
21. M. Gao, L. Zhu, C. K. Peh, G. W. Ho, Solar absorber material and system designs for photothermal water vaporization towards clean water and energy production. *Energ. Environ. Sci.* **12**, 841–864 (2018).
22. Y. Shi, C. Zhang, R. Li, S. Zhuo, Y. Jin, L. Shi, S. Hong, J. Chang, C. Ong, P. Wang, Solar evaporator with controlled salt precipitation for zero liquid discharge desalination. *Environ. Sci. Technol.* **50**, 11822–11830 (2018).
23. G. Xue, K. Liu, Q. Chen, P. Yang, J. Li, T. Ding, J. Duan, B. Qi, J. Zhou, Robust and low-cost flame-treated wood for high-performance solar steam generation. *ACS Appl. Mater. Interfaces* **9**, 15052–15057 (2017).
24. H.-N. Kim, S. Vahidinia, A. L. Holt, A. M. Sweeney, S. Yang, Geometric design of scalable forward scatterers for optimally effcient solar transformers. *Adv. Mater.* **29**, 1702922 (2017).
25. O. Neumann, C. Feronti, A. D. Neumann, A. Dong, K. Schell, B. Lu, E. Kim, M. Quinn, S. Thompson, N. Grady, P. Nordlander, M. Oden, N. J. Halas, Compact solar autoclave based on steam generation using broadband light-harvesting nanoparticles. *Proc. Natl. Acad. Sci. U.S.A.* **110**, 11677–11681 (2013).
26. C. Ma, J. Yan, Y. Huang, C. Wang, G. Yang, The optical duality of tellurium nanoparticles for broadband solar energy harvesting and efficient photothermal conversion. *Sci. Adv.* **4**, eaas9894 (2018).
27. T. Li, M. Zhu, Z. Yang, J. Song, J. Dai, Y. Yao, W. Luo, G. Pastel, B. Yang, L. Hu, Wood composite as an energy efficient building material: Guided sunlight transmittance and effective thermal insulation. *Adv. Energy Mater.* **6**, 1601122 (2016).
28. H. Ren, M. Tang, B. Guan, K. Wang, J. Yang, F. Wang, M. Wang, J. Shan, Z. Chen, D. Wei, H. Peng, Z. Liu, Hierarchical graphene foam for efficient omnidirectional solar-thermal energy conversion. *Adv. Mater.* **29**, 1702590 (2017).
29. Y. Yang, R. Zhao, T. Zhang, K. Zhao, P. Xiao, Y. Ma, P. M. Ajayan, G. Shi, Y. Chen, Graphene-based standalone solar energy converter for water desalination and purification. *ACS Nano* **12**, 829–835 (2018).
30. P. Zhang, J. Li, L. Lv, Y. Zhao, L. Qu, Vertically aligned graphene sheets membrane for highly efficient solar thermal generation of clean water. *ACS Nano* **11**, 5087–5093 (2017).
31. N. Xu, X. Hu, W. Xu, X. Li, L. Zhou, S. Zhu, J. Zhu, Mushrooms as efficient solar steam-generation devices. *Adv. Mater.* **29**, 1606762 (2017).
32. P. Zhang, F. Liu, Q. Liao, H. Yao, H. Geng, H. Cheng, C. Li, L. Qu, A microstructured graphene/poly(*N*-isopropylacrylamide) membrane for intelligent solar water evaporation. *Angew. Chem. Int. Ed.* **57**, 16343–16347 (2018).
33. X. Gao, H. Ren, J. Zhou, R. Du, C. Yin, R. Liu, H. Peng, L. Tong, Z. Liu, J. Zhang, Synthesis of hierarchical graphdiyne-based architecture for efficient solar steam generation. *Chem. Mater.* **29**, 5777–5781 (2017).
34. C. Finnerty, L. Zhang, D. L. Sedlak, K. L. Nelson, B. Mi, Synthetic graphene oxide leaf for solar desalination with zero liquid discharge. *Environ. Sci. Technol.* **51**, 11701–11709 (2017).
35. G. Ni, S. H. Zandavi, S. M. Javid, S. V. Boriskina, T. A. Cooper, G. Chen, A salt-rejecting floating solar still for low-cost desalination. *Energ. Environ. Sci.* **11**, 1510–1519 (2018).
36. W. Xu, X. Hu, S. Zhuang, Y. Wang, X. Li, L. Zhou, S. Zhu, J. Zhu, Flexible and salt resistant janus absorbers by electrospinning for stable and efficient solar desalination. *Adv. Energy Mater.* **8**, 1702884 (2018).
37. T. A. Cooper, S. H. Zandavi, G. W. Ni, Y. Tsurimaki, Y. Huang, S. V. Boriskina, G. Chen, Contactless steam generation and superheating under one sun illumination. *Nat. Commun.* **9**, 5086 (2018).
38. E. Garnett, P. Yang, Light trapping in silicon nanowire solar cells. *Nano Lett.* **10**, 1082–1087 (2010).
39. Y. Xia, X. Pu, J. Liu, J. Liang, P. Liu, X. Li, X. Yu, CuO nanoleaves enhance the c-Si solar cell efficiency. *J. Mater. Chem. A* **2**, 6796–6800 (2014).
40. N. Miljkovic, R. Enright, Y. Nam, K. Lopez, N. Dou, J. Sack, E. N. Wang, Jumping-droplet-enhanced condensation on scalable superhydrophobic nanostructured surfaces. *Nano Lett.* **13**, 179–187 (2013).

41. World Health Organization (WHO), Safe Drinking-Water from Desalination (WHO, 2011); http://apps.who.int/iris/bitstream/10665/70621/1/WHO_HSE_WSH_11.03_eng.pdf.
42. Ministry of Ecology and Environment of the People's Republic of China, Water-Pollutant-Emission-Standard; http://kjs.mep.gov.cn/hjbhbz/bzwb/shjbh/swrwpfbz/.
43. W. A. Hovis, Infrared spectral reflectance of some common minerals. *Appl. Optics* **5**, 245–248 (1966).

Acknowledgments: We acknowledge the micro-fabrication center of the National Laboratory of Solid State Microstructures (NLSSM) for technique support and the Jiangsu Donghai Silicon Industry Science and Technology Innovation Center. **Funding:** This work was jointly supported by the National Key Research and Development Program of China (grant no. 2017YFA0205700), the State Key Program for Basic Research of China (grant no. 2015CB659300), the National Natural Science Foundation of China (grant nos. 21805132, 11574143, 11874211, 11621091, and 61735008), the Natural Science Foundation of Jiangsu Province (grant no. BK20180341), and the Fundamental Research Funds for the Central Universities (grant nos. 021314380150 and 021314380140). **Author contributions:** J.Z., N.X., and J.L. conceived and planned this research; N.X. and J.L. did the experiments; N.X., J.L., Yang Wang, C.F., X.L., Yuxi Wang, L.Z., B.Z., Z.W., and S.Z. performed data analysis; J.Z., N.X., J.L., and S.Z. wrote the manuscript. All authors discussed the results and approved the final version of the manuscript. **Competing interests:** The authors declare that they have no competing interests. **Data and materials availability:** All data needed to evaluate the conclusions in the paper are present in the paper and/or the Supplementary Materials. Additional data related to this paper may be requested from the authors.

Submitted 17 January 2019
Accepted 30 May 2019
Published 5 July 2019
10.1126/sciadv.aaw7013

Citation: N. Xu, J. Li, Y. Wang, C. Fang, X. Li, Y. Wang, L. Zhou, B. Zhu, Z. Wu, S. Zhu, J. Zhu, A water lily–inspired hierarchical design for stable and efficient solar evaporation of high-salinity brine. *Sci. Adv.* **5**, eaaw7013 (2019).

Science Advances

A water lily–inspired hierarchical design for stable and efficient solar evaporation of high-salinity brine

Ning Xu, Jinlei Li, Yang Wang, Chang Fang, Xiuqiang Li, Yuxi Wang, Lin Zhou, Bin Zhu, Zhen Wu, Shining Zhu and Jia Zhu

Sci Adv **5** (7), eaaw7013.
DOI: 10.1126/sciadv.aaw7013